Applied Physics Letters

# Anisotropic epsilon-near-pole (ENP) resonance leads to hyperbolic photonic dispersion in homologous $(Bi_2)_m(Bi_2Se_3)_n$ topological quantum materials

Cite as: Appl. Phys. Lett. **119**, 011902 (2021); https://doi.org/10.1063/5.0053587
Submitted: 09 April 2021 . Accepted: 17 June 2021 . Published Online: 06 July 2021

Krishna Chand Maurya, Animesh Bhui, Kanishka Biswas, and Bivas Saha

Applied Physics Letters ARTICLE scitation.org/journal/apl

# Anisotropic epsilon-near-pole (ENP) resonance leads to hyperbolic photonic dispersion in homologous $(Bi_2)_m(Bi_2Se_3)_n$ topological quantum materials

Cite as: Appl. Phys. Lett. **119**, 011902 (2021); doi: 10.1063/5.0053587
Submitted: 9 April 2021 · Accepted: 17 June 2021 ·
Published Online: 6 July 2021

View Online Export Citation CrossMark

Krishna Chand Maurya,[1,2,3] Animesh Bhui,[4] Kanishka Biswas,[2,3,4] and Bivas Saha[1,2,3,a)]

## AFFILIATIONS

[1]Chemistry and Physics of Materials Unit, Jawaharlal Nehru Centre for Advanced Scientific Research, Bangalore 560064, India
[2]International Centre for Materials Science, Jawaharlal Nehru Centre for Advanced Scientific Research, Bangalore 560064, India
[3]School of Advanced Materials, Jawaharlal Nehru Centre for Advanced Scientific Research, Bangalore 560064, India
[4]New Chemistry Unit, Jawaharlal Nehru Centre for Advanced Scientific Research, Bangalore 560064, India

[a)]**Author to whom correspondence should be addressed:** bsaha@jncasr.ac.in and bivas.mat@gmail.com

## ABSTRACT

The hyperbolic iso-frequency surface (dispersion) of photons in materials that arise from extreme dielectric anisotropy is the latest frontier in nanophotonics with potential applications in subwavelength imaging, coherent thermal emission, photonic density of state engineering, negative refraction, thermal hyperconductivity, etc. Most hyperbolic materials utilize nanoscale periodic metal/dielectric multilayers (superlattices) or metallic nanowires embedded inside the dielectric matrix that require expensive growth techniques and possess significant fabrication challenges. Naturally occurring bulk materials that exhibit tunable hyperbolic photonic dispersion in the visible-to-near-IR spectral ranges will, therefore, be highly beneficial for practical applications. Due to the layered structure and extreme anisotropy, a homologous series of $(Bi_2)_m(Bi_2Se_3)_n$ could serve as a unique class of natural hyperbolic material with tunable properties derived from different stoichiometry. In this Letter, we demonstrate hyperbolic photonic dispersion in a single crystal of weak topological insulator BiSe ($m = 1$ and $n = 2$), where a $Bi_2$ layer is inserted between $Bi_2Se_3$ ($m = 0$ and $n = 1$) quintuple layers in the visible (525–710 nm) and near-UV (210–265 nm) spectral range. The origin of hyperbolic dispersion in homologous $(Bi_2)_m(Bi_2Se_3)_n$ topological quantum materials arises from their anisotropic epsilon-near-pole resonance corresponding to the interband transitions that lead to different signs of its dielectric permittivity. The tunability of hyperbolic dispersion is further demonstrated by alloying $Bi_2Se_3$ with Mn that alters the interband transition positions and expands their hyperbolic spectral regime from 500–1045 to 500–1185 nm.



Hyperbolic materials (HMs) are indefinite media with the dielectric permittivity of opposite signs in the principal components of the dielectric tensor.[1–3] Due to the strong structural anisotropy, HMs act as metals in one direction characterized by the negative real component of dielectric permittivity ($\varepsilon_1$), while along the other orthonormal directions, they act as dielectrics with positive $\varepsilon_1$.[3,4] Such an exotic direction-dependent optical response in HMs leads to the photonic hyperbolic dispersion of their iso-frequency surfaces for the transverse-magnetic (TM) (extraordinary) wave,[4] and several unique applications, such as subwavelength imaging,[5] negative refraction, super-Planckian heat transfer,[6] and control of single-photon emitters,[7,8] have been proposed and demonstrated. Most implementations of HMs in the visible-to-near-IR spectral range utilize artificially structured metal/dielectric multilayers and superlattices with noble metals (e.g., Au, Ag) and oxide dielectrics (e.g., $Al_2O_3$, $TiO_2$) as well as transition metal nitride as components, such as $Ag/TiO_2$[9] and $Au/Al_2O_3$[10] multilayers and epitaxial $TiN/Al_{1-x}Sc_xN$ superlattices.[11] In addition, metallic nanowires embedded inside the dielectric matrix are also developed that exhibit hyperbolic dispersion in the visible spectral range.[12–14] Multilayer/superlattices and nanocomposites, however, involve expensive and complex growth techniques and present various fabrication challenges that limit the exploration of their exotic functional properties and device realization. Therefore, naturally occurring bulk materials that exhibit HM properties with a broad spectral range will be greatly beneficial.[15]

Bi-chalcogenides belong to a family of materials known as tetradymites with the formula $M_2X_3$, where M = Bi, Sb and X = S, Se, Te,

and have drawn significant interest in recent years for topological insulating properties owing to their interesting metallic surface states. These materials are also attractive for high thermoelectric figures-of-merit (ZT) for solid-state waste-heat recovery and cooling applications.[16] Like other tetradymites, Bi-chalcogenides, such as $Bi_2Se_3$, exhibit a layered structure with atomic monolayers that arrange themselves into hexagonal quintuple layers [see Fig. 1(c)].[17] A weak van der Waals interaction exists between the layers in such tetradymites that is akin to graphene or other layer 2D materials, such as $MoS_2$ and $MoTe_2$. Due to the extreme structural anisotropy (strong in-plane bonds with a heavy ionic character and weak cross-plane van der Waals interaction), tetradymites are expected to exhibit strong anisotropic dielectric permittivity and even hyperbolic photonic iso-frequency surfaces. Indeed, bulk $Bi_2Se_3$ single crystals have recently demonstrated both the type-I and type-II hyperbolic dispersions in the ultraviolet (UV)-to-visible spectral ranges.[18] In addition, for the large-scale demonstration of the homologous $(Bi_2)_m(Bi_2Se_3)_n$ series as a potential anisotropic optical medium, it is necessary that more members of this family exhibit hyperbolic iso-frequency surfaces and that the spectral range of their hyperbolic dispersion is tuned with the incorporation of foreign atoms.

BiSe is the latest entrant to the Bi-chalcogenides class of materials and belongs to the same homologous series $(Bi_2)_m(Bi_2Se_3)_n$, where $m = 1$ and $n = 2$.[19] BiSe has emerged as an interesting weak topological insulator and exhibits a layered crystal structure with a bismuth bilayer ($Bi_2$) sandwiched between two $Bi_2Se_3$ quintuples (Se–Bi–Se–Bi–Se) layers [see Fig. 1(c)].[20] Due to the soft localized vibration of bismuth layers inside BiSe that couples with the heat carrying acoustic phonon, BiSe exhibits about three times smaller thermal conductivity compared to the $Bi_2Se_3$ and a high overall thermoelectric figure-of-merit (ZT) of 0.8 at 425 K.[21] Angle resolved photoemission measurements on BiSe have also demonstrated Rashba states that closely agree with theoretically predicted weak topological insulating properties.[19] Therefore, it is natural to measure the anisotropic dielectric permittivity in BiSe and explore its HM properties. In this work, photon energy ($E$) dependent anisotropic dielectric permittivity of BiSe and $Bi_2Se_3$ is measured along and perpendicular to the *ab*-plane with spectroscopic ellipsometry that shows their hyperbolic nature in the UV to the visible spectral range. Through a detailed analysis of experimental results and its comparison with the band structure, we show that the origin of the hyperbolic dispersion in BiSe, $Bi_2Se_3$, and Bi-chalcogenides, in general, originates from the anisotropic epsilon-near-pole (ENP) resonance[22,23] corresponding to the interband transitions. In addition, the spectral range of hyperbolic dispersion is tuned in $Bi_2Se_3$ from 500–1045 to 500–1185 nm by doping Mn in the Bi-atomic sites that alter its interband transition energy positions and carrier concentrations.[24] $Bi_2Se_3$ was chosen for the tunability of hyperbolic spectral range since Mn doping at Bi-sites in $Bi_2Se_3$ is expected to produce a uniform layered solid solution, while Mn-doping in BiSe will alter the metallic $Bi_2$-layer that is crucial for its heterostructure nature.

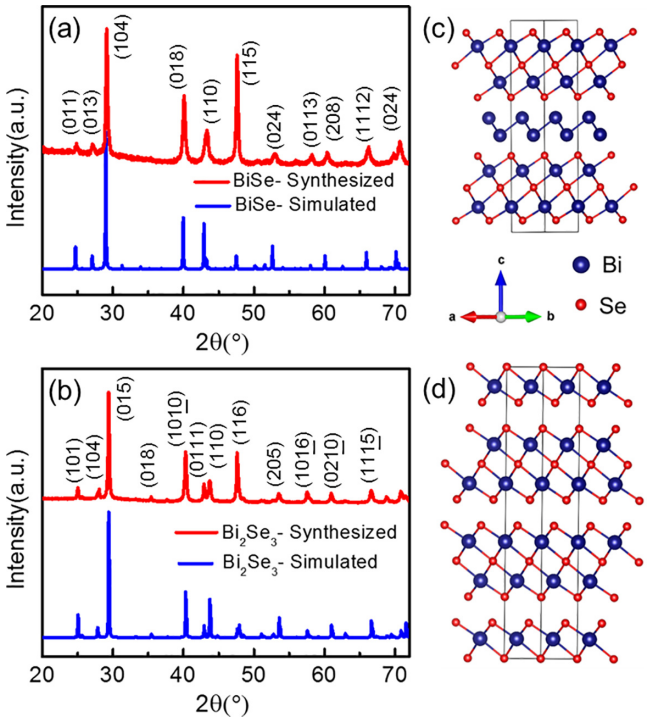


**FIG. 1.** Powder x-ray diffractogram of as-synthesized (red line) and simulated (blue line) (a) BiSe and (b) $Bi_2Se_3$ crystals is presented. The crystal structure of (c) BiSe and (d) $Bi_2Se_3$ is shown. Blue and red atoms represent Bi and Se atoms, respectively, in the BiSe and $Bi_2Se_3$ layers.

BiSe and $Bi_2Se_3$ single crystals are synthesized by a modified Bridgman method, where the stoichiometric mixture of high purity Bi and Se is sealed in quartz ampules and annealed at high temperatures (see the supplementary material for details about the synthesis). $Bi_xMn_{2-x}Se_3$ crystals are further obtained by mixing an appropriate amount of Mn with Bi and Se and following the same synthesis technique. A Bruker D8 diffractometer with Cu K$\alpha$1 ($\lambda = 1.540\,59$ Å) radiation was utilized to collect the powder-XRD pattern of the crystals. Hall measurements are performed to obtain the electrical conductivity, carrier concentration, and mobility of the pristine as well as doped crystals at room temperature. Optical properties are measured with a variable angle spectroscopic ellipsometer (RC-2 J.A. Woollam Co.) in the range from 210 to 2500 nm in the reflection mode at three different angles (55°, 65°, and 75°) of incidence. The experimental [Psi ($\psi$), Delta ($\Delta$)] spectrum is modeled with a uniaxial anisotropy model. Details on the structure and electrical characterization, ellipsometry measurements and data fitting are presented in supplementary material Sec. 3.

Power x-ray diffraction pattern of the as-synthesized compounds could be indexed as layered BiSe [space group $P\bar{3}m1$, Fig. 1(a)] and $Bi_2Se_3$ [space group $R\bar{3}m$, Fig. 1(b)]. Phase purity of the BiSe and $Bi_2Se_3$ was confirmed via the absence of any impurity peaks. Despite the similarity in the powder XRD pattern of BiSe and $Bi_2Se_3$ due to the basic quintuple layered structure, the presence of extra $Bi_2$ bilayer in BiSe slightly changes the peak position of (hkl) reflections.[25]

Spectroscopic ellipsometry characterization reveals that BiSe exhibits both type-I ($\varepsilon_{1,zz} < 0$ and $\varepsilon_{1,xx} > 0$) and type-II ($\varepsilon_{1,zz} > 0$ and $\varepsilon_{1,xx} < 0$) hyperbolic dispersion [see Fig. 2(d)] in the visible and near-UV spectral ranges, respectively. For the near-IR spectral regime (~710 to 2500 nm), both the in-plane ($\varepsilon_{1,xx}$) and cross-plane ($\varepsilon_{1,zz}$) real components of the dielectric constant of BiSe are found to be positive that represent its dielectric nature with closed iso-frequency surfaces (see Fig. 2). As BiSe is inherently a low-bandgap

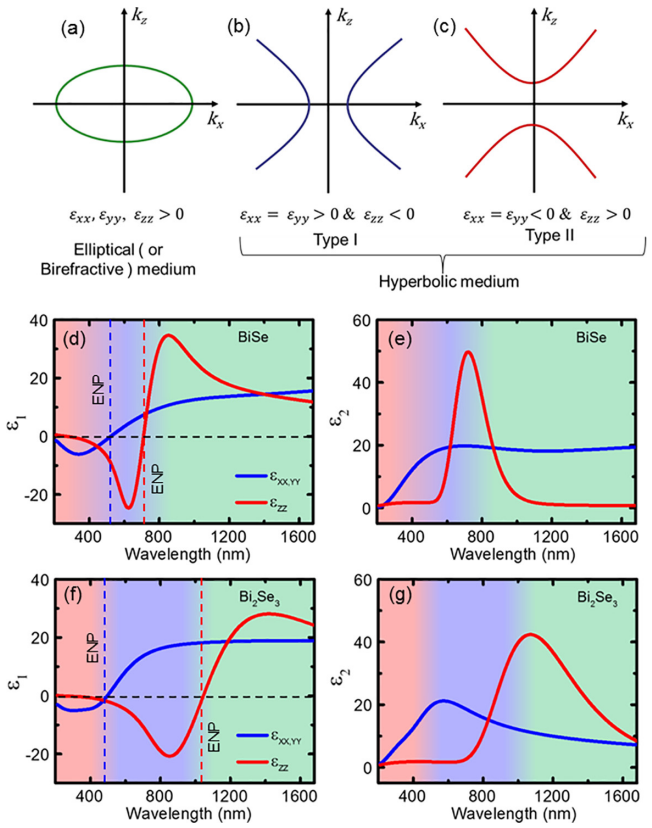


**FIG. 2.** Schematic diagram of iso-frequency surfaces in momentum space for elliptical (a), hyperbolic type-I (b), and type-II (c) medium. The anisotropic optical behavior of the homologous $(Bi_2)_m(Bi_2Se_3)_n$ heterostructure family. The real [$\varepsilon_1$, (d) and (f)] and imaginary [$\varepsilon_2$, (e) and (g)] parts of the dielectric permittivity. The blue and red lines represent the values for the in-plane and cross-plane direction. The different background color represents different medium, such as green: elliptical, blue: hyperbolic type-I, red: hyperbolic type-II. $Bi_2Se_3$ and BiSe show the type-I hyperbolic nature in 500–1040 and 525–710 nm wavelength ranges, respectively.

semiconductor[19] (theoretically calculated gap of ∼42 meV) with a bulk carrier concentration of $2.6 \times 10^{19}$ cm$^{-3}$, free-electron or Drude absorption that is usually dominant in the near-IR spectral range is quite small and results in its positive dielectric constants. However, as the wavelength decreases, BiSe exhibits a clear transition of its photonic iso-frequency surface from elliptic-to-hyperbolic with $\varepsilon_{1,zz}$ exhibiting negative values, while the $\varepsilon_{1,xx}$ remains positive. This transition from positive-to-negative $\varepsilon_{1,zz}$ at 710 nm in BiSe results from the optical excitation due to interband transitions as evidenced by a peak in the loss function (LF) ($-\mathrm{Im}\,[1/\varepsilon] = \frac{\varepsilon_1(\omega)}{\varepsilon_1^2(\omega)+\varepsilon_2^2(\omega)}$)[26,27] (see the supplementary material for details). Such an optical response of BiSe is representative of the type-I hyperbolic dispersion and ranged a large portion of the visible spectrum from 525 to 710 nm. A further decrease in the wavelength initially results a metallic-like region with both $\varepsilon_{1,zz}$ and $\varepsilon_{1,xx}$ exhibiting negative values from 525 to 265 nm and subsequent type-II hyperbolic dispersion in the spectral range from 265 to 210 nm with $\varepsilon_{1,zz} > 0$ and $\varepsilon_{1,xx} < 0$. $\varepsilon_{1,xx}$ of BiSe is found to undergo the positive-to-negative transition at ∼525 nm, and a sharp rise in the LF represents its optical excitation character due to interband transitions.

Similar to BiSe, the $Bi_2Se_3$ crystal also exhibits the hyperbolic photonic dispersion with both type-I ($\varepsilon_{1,zz} < 0$ and $\varepsilon_{1,xx} > 0$) and type-II ($\varepsilon_{1,zz} > 0$ and $\varepsilon_{1,xx} < 0$) characteristics having a spectral range of 500–1040 and 210–230 nm, respectively. Above 1040 nm, in the near-IR spectral range, both $\varepsilon_{1,zz}$ and $\varepsilon_{1,xx}$ of $Bi_2Se_3$ are also found to be positive that represents its optical dielectric nature. Similarly, the $\varepsilon_{1,zz}$ and $\varepsilon_{1,xx}$ undergo a positive-to-negative transition at 1040 and 500 nm, respectively, due to interband transitions characterized by peaks in their LFs. It is interesting to note that the $\varepsilon_{1,xx}$'s transition from positive to negative in BiSe as well as in $Bi_2Se_3$ is almost at the same spectral position, while the $\varepsilon_{1,zz}$ transition defers significantly for reasons discussed subsequently. Overall, the spectral positions as well as the nature of the dielectric permittivity obtained in $Bi_2Se_3$ crystals in this study are consistent with the previous reports of its anisotropic dielectric permittivity. While in the previous work, the hyperbolic dispersion was found to span 700–1180 nm,[18] in this work the spectral range is found from 500 to 1040 nm possibly due to the difference in the sample quality.

To understand the origin of the hyperbolic dispersion in BiSe and $Bi_2Se_3$, a detailed analysis has been performed. Unlike the conventional demonstrations of hyperbolic metamaterials (HMMs) in the UV-to-visible spectral range that utilizes metals with high carrier densities in the multilayers/superlattices or the nanowires, the origin of the hyperbolic dispersion in BiSe, $Bi_2Se_3$, and Bi-chalcogenides, in general, is significantly different. As the Bi-chalcogenides exhibit low carrier concentrations, the free-electron or Drude contribution in the entire UV-visible to the near-IR spectral range is rather low and the $\varepsilon_1$ never reached negative values from Drude contributions only. For noble metals[28] as well as in metallic nitrides,[29,30] high carrier concentrations almost always lead to negative $\varepsilon_1$ in the near-IR spectral range and results in hyperbolic dispersions in metal/dielectric multilayers/superlattices as well as in embedded metallic nanowires inside the dielectric matrix. Instead, the interband transition in Bi-chalcogenides in the visible and near IR spectral region leads to the Gaussian like dielectric response[31] accompanied by an effective epsilon-near-pole (ENP) (marked in Fig. 2) and negative permittivity. In a lossless medium, an ideal pole of the dielectric constant leads to $\varepsilon_1 \rightarrow (\pm)\infty$.[22,23] The addition of losses, however, regularizes the singularity, reduces impedance mismatch, and leads to the enhanced absorption in a narrow spectral region. Since the Bi-chalcogenides exhibit an inherent structural anisotropy with direction-dependent energy-vs-momentum (E-vs-$\kappa$) relationships, the spectral position of the interband transition and ENP for the in-plane and cross-plane directions are shifted. This shift in ENP leads to different signs of its dielectric permittivity within a band of wavelength and, hence, results in the hyperbolic dispersion.

For BiSe, it is clear that the ENP along the cross-plane direction occurs at ∼710 nm accompanied by a peak in the imaginary component of the dielectric permittivity ($\varepsilon_2$), while the ENP along the in-plane direction is found at ∼525 nm with its associated peak in the $\varepsilon_2$. This difference in the ENP leads to its hyperbolic type-I dispersion in the 525–710 nm. The $\varepsilon_{2,zz}$ peak intensity is quite larger compared to the $\varepsilon_{2,xx}$, and the full-width-at-the-half-maxima (FWHM) of the former peak is much smaller compared to a much broader peak in $\varepsilon_{2,xx}$ that show a stronger cross-plane interband transition resonance than

that along the in-plane direction. The ENP for the $Bi_2Se_3$ along the cross-plane and in-plane directions is found at 1040 and 500 nm, respectively, that leads to its type-I hyperbolic nature with associated peaks in the optical loss ($\varepsilon_2$) spectrum. The nature of the peak intensity and FWHM for the $\varepsilon_{2,zz}$ and $\varepsilon_{2,xx}$ in $Bi_2Se_3$ is again consistent with the previous report.

In order to gain an insight into the nature of the interband transitions in Bi-chalcogenides, the results obtained here are further compared with their electronic structure. As $Bi_2Se_3$ is a well-established topological insulator and thermoelectric material, a large volume of well-defined electronic structure calculations is available in the literature.[17,32] Careful analysis reveals that both the valence band maxima (VBM) and the conduction band minima (CBM) in $Bi_2Se_3$ are located at the Γ-point of the Brillouin zone leading to an energy gap of 0.35 eV. However, for the relevant interband transition observed in the present as well as in the previous HM studies, the second and third conduction bands at the Γ-point are found to be more important. The energy separation between the valence band maxima and the second and third conduction bands at the Γ-point are found to be ∼1.2 (1033) and 2.40 eV (516 nm), respectively,[32] that are close to the measured ENP points found in the optical measurements. While the energy separation is measured at the Γ-point, the strength of the interband transitions along the in-plane (Γ–L) and cross-plane (Γ–Z) directions can be determined by the joint density of states[33] [see Eq. (1)] due to differences in the curvature of the bands along the two directions

$$\rho_{cv}(h\omega) = \frac{2}{8\pi^3}\int\int \frac{ds}{|\nabla_k (E_c - E_v)|_{E_c - E_v = h\omega}}. \quad (1)$$

While a detailed calculation is beyond the scope of the present study, it is apparent from the band structure as well as from the optical characterization that, for the cross-plane (Γ–Z) directions, the interband transition at 1.1 eV (1127 nm) will be dominant, while for the in-plane (Γ–L) direction, the transition at 2.45 eV (506 nm) will lead.[32] This conclusion is also supported by the facts that (a) along the in-plane direction, atoms in $Bi_2Se_3$ are bound together by stronger ionic bonds, while along the cross-plane direction, weak van der Waals interaction prevails that presumably leads to much stronger in-plane coupling and interband transitions than weaker cross-plane coupling and interband transition, and (b) the $\varepsilon_{1,xx}$ ENP for the $Bi_2Se_3$ and BiSe is found to be approximately at the same spectral position since along the in-plane direction they resemble similar compared to the cross-plane directions. For the BiSe, the electronic structure calculations have not evolved as much as it is the case for $Bi_2Se_3$, and the comparison between the experimental band structure and theoretical calculations remains for future avenue of research.

The tunability of the hyperbolic dispersion spectral range in Bi-chalcogenides is further demonstrated with Mn-doping in Bi-sites in $Bi_2Se_3$ as a model system for reasons explained in the introduction. Results reveal that the incorporation of Mn acts as a hole dopant (*p*-type dopant) in $Bi_2Se_3$ and reduces its carrier concentration. While pristine-$Bi_2Se_3$ exhibited a carrier concentration of $1.8 \times 10^{19}$ cm$^{-3}$, the incorporation of 15% and 20% Mn in $Bi_2Se_3$ reduced the carrier concentration to $1.0 \times 10^{19}$ and $6.4 \times 10^{18}$ cm$^{-3}$, respectively. Importantly, the incorporation of acceptor states close to the valence band edges in $Bi_2Se_3$ reduced the cross-plane interband transition energy from ∼1.19 eV (1040 nm) in pure $Bi_2Se_3$ to ∼1.12 eV (1100 nm) for $Bi_{1.85}Mn_{0.15}Se_3$ and 1.04 eV (1185 nm) for $Bi_{1.80}Mn_{0.20}Se_3$. The shift in ENP resonance positions is also captured in the peaks at the optical loss ($\varepsilon_{2,zz}$) spectrum as well as in the LF (See Fig. 3). Interestingly, the interband transition positions along the in-plane direction of the $Bi_{1.85}Mn_{0.15}Se_3$ and $Bi_{1.80}Mn_{0.20}Se_3$ did not change significantly compared to the pristine-$Bi_2Se_3$ (Fig. 3). As a result, the type-I hyperbolic

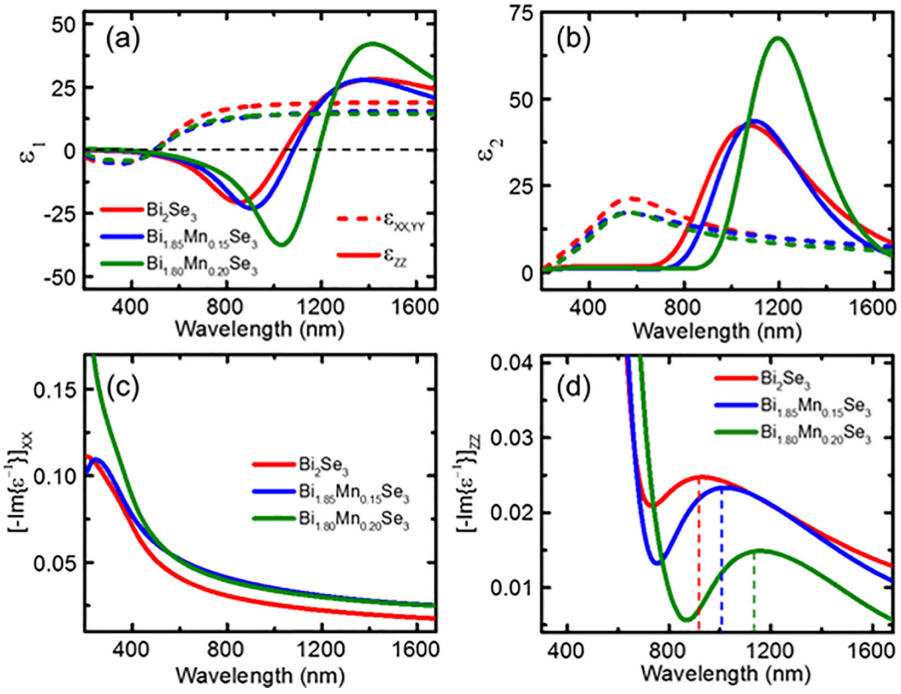


**FIG. 3.** Tunable hyperbolic nature of $Bi_2Se_3$. The hyperbolic range shows a red shift by Mn doping in $Bi_2Se_3$. The real [$\varepsilon_1$, (a)] and imaginary [$\varepsilon_2$, (b)] parts of the dielectric permittivity of Mn doped $Bi_2Se_3$ or $Bi_{2-x}Mn_xSe_3$ (x = 0.15, 0.2). Calculated loss function for (c) in-plane and (d) cross-plane directions of $Bi_{2-x}Mn_xSe_3$ (x = 0.15, 0.2) that shows redshift along *c*-axis with Mn content increment.

dispersion range in $Bi_{1.85}Mn_{0.15}Se_3$ and $Bi_{1.80}Mn_{0.20}Se_3$ spanned from 500 to 1040 and from 500 to 1185 nm, respectively.

Having demonstrated the origin and tunability of hyperbolic dispersion in BiSe, $Bi_2Se_3$, we now attempt to contextualize their hyperbolic spectral range with other natural hyperbolic materials. As discussed earlier, apart from the subwavelength photonics, there is a wide range of applications, such as solar energy harvesting,[34] bio-photonics,[35] telecommunication,[36] optical clocks,[37] frequency comb,[38] where the hyperbolic material can be useful. Obviously, one material can be useful not only for all types of application because the different applications have different requirements, for example, the materials with high optical loss ($\varepsilon_2$) are useful for the confinement and impedance effects,[39] such as loss-induced heating,[40] plasmon-induced hot carrier,[41] electro-thermo-plasmonic nanotweezer,[42] but also for propagation, such as optical nanocircuits,[43] photon tunneling,[44,45] supercoupling,[46] $\varepsilon_2$ should be very low (ideally zero). Also, different applications operate in the different electromagnetic spectrum, so there is plenty of room to discover modern natural hyperbolic materials. Finally, we have plotted the hyperbolic region for BiSe, $Bi_2Se_3$, and $Bi_{2-x}Mn_xSe_3$ with the previously reported natural hyperbolic material, such as $Bi_2Te_3$,[18] graphite,[47] hBN,[48] $MgB_2$,[49] $Sr_2RuO_4$,[49] $La_{1.92}Sr_{0.08}CuO_4$,[49] as shown in Fig. 4. $(Bi_2)_m(Bi_2Se_3)_n$ has the hyperbolic region in the UV to near-infrared (NIR) range, which can be useful in solar energy harvesting, bio-photonics, etc.

In conclusion, we demonstrate both type-I (525–710 nm) and type-II (210–265 nm) hyperbolic photonic dispersion in bulk weak topological insulator BiSe, where the $Bi_2$-layer is sandwiched between $Bi_2Se_3$ quintuple layers. We show that, unlike conventional hyperbolic materials where metals with high carrier densities are used to achieve free carriers or Drude absorption and negative permittivity, hyperbolic dispersion in the homologous $(Bi_2)_m(Bi_2Se_3)_n$ series, in general, arises from direction-dependent interband transition and associated epsilon-near-pole (ENP) resonances. The spectral position of the ENP was tuned by doping Mn in Bi-atomic sites that alter the interband transition energy and, hence, type-I hyperbolic spectral range. The demonstration of BiSe as a hyperbolic photonic medium and elucidation of its origin will not only expand their exploration for function optical materials and devices but also enable the demonstration of exotic optical properties without the need for expensive growth and nanofabrication techniques.

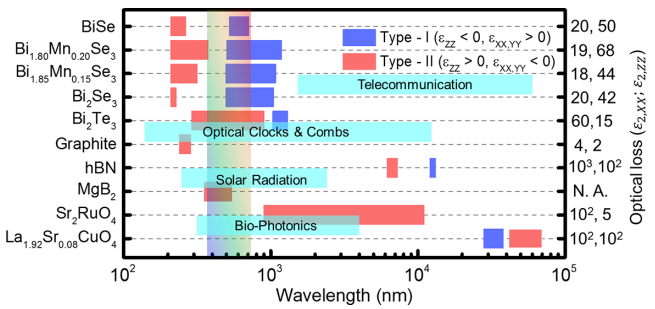


**FIG. 4.** Hyperbolic wavelength bands in natural materials. Blue and orange colors correspond to the bands with type-I and type-II hyperbolic medium, respectively. The top four lines (BiSe, $Bi_2Se_3$, and Mn doped $Bi_2Se_3$) represent that the hyperbolic materials are compared with other well-known natural hyperbolic material. The vertical "spectrum bar" indicates the wavelength range corresponding to visible light. The horizontal bar indicates the wavelength range for the application. The y-scale at the right side indicates the maximum optical loss along in-plane and the cross-plane ($\varepsilon_{2,xx}$ and $\varepsilon_{2,zz}$) directions, respectively.

See the supplementary material for information related to the sample preparation, XRD measurement, ellipsometer measurements and data fitting, and loss function analysis.

K.C.M. and B.S. acknowledge support from the International Centre for Materials Science (ICMS) and Sheikh Saqr Laboratory (SSL) of the Jawaharlal Nehru Centre for Advanced Scientific Research (JNCASR). B.S. acknowledges the Young Scientist Research Award (YSRA) from the Board of Research in Nuclear Sciences (BRNS), Department of Atomic Energy (DAE), India, under Grant No. 59/20/10/2020-BRNS/59020 for financial support. K.C.M. and A.B. thank the CSIR for the fellowship. K.B. acknowledges SERB (No. CRG/2019/001306) and Swarnajayanti fellowship, Department of Science & Technology (DST) (No. DST/SJF/CSA-02/2018-19), India.

## DATA AVAILABILITY

The data that support the findings of this study are available from the corresponding author upon reasonable request.

## REFERENCES

[1]D. R. Smith and D. Schurig, Phys. Rev. Lett. **90**, 077405 (2003).
[2]M. A. Noginov, Y. A. Barnakov, G. Zhu, T. Tumkur, H. Li, and E. E. Narimanov, Appl. Phys. Lett. **94**, 151105 (2009).
[3]Z. Guo, H. Jiang, and H. Chen, J. Appl. Phys. **127**, 071101 (2020).
[4]A. Poddubny, I. Iorsh, P. Belov, and Y. Kivshar, "Hyperbolic metamaterials," Nat. Photonics **7**, 948–957s (2013).
[5]Z. Liu, H. Lee, Y. Xiong, C. Sun, and X. Zhang, Science **315**, 1686 (2007).
[6]Y. Guo, L. Cortes, S. Molesky, and Z. Jacob, Appl. Phys. Lett. **101**, 131106 (2012).
[7]W. D. Newman, C. L. Cortes, and Z. Jacob, J. Opt. Soc. Am. B **30**, 766 (2013).
[8]M. Y. Shalaginov, V. V. Vorobyov, J. Liu, M. Ferrera, A. V. Akimov, A. Lagutchev, A. N. Smolyaninov, V. V. Klimov, J. Irudayaraj, A. V. Kildishev, A. Boltasseva, and V. M. Shalaev, Laser Photonics Rev. **9**, 120 (2015).
[9]G. Subramania, A. J. Fischer, and T. S. Luk, Appl. Phys. Lett. **101**, 241107 (2012).
[10]K. V. Sreekanth, T. Biaglow, and G. Strangi, J. Appl. Phys. **114**, 134306 (2013).
[11]B. Saha, G. V. Naik, S. Saber, C. Akatay, E. A. Stach, V. M. Shalaev, A. Boltasseva, and T. D. Sands, Phys. Rev. B **90**, 125420 (2014).
[12]R. Chandrasekar, Z. Wang, X. Meng, S. I. Azzam, M. Y. Shalaginov, A. Lagutchev, Y. L. Kim, A. Wei, A. V. Kildishev, A. Boltasseva, and V. M. Shalaev, ACS Photonics **4**, 674 (2017).
[13]P. Guo, R. P. H. Chang, and R. D. Schaller, Appl. Phys. Lett. **111**, 021108 (2017).
[14]B. D. F. Casse, W. T. Lu, Y. J. Huang, E. Gultepe, L. Menon, and S. Sridhar, Appl. Phys. Lett. **96**, 023114 (2010).
[15]E. E. Narimanov and A. V. Kildishev, Nat. Photonics **9**, 214 (2015).
[16]J. P. Heremans, R. J. Cava, and N. Samarth, Nat. Rev. Mater. **2**, 17049 (2017).
[17]J. Chang, L. F. Register, and S. K. Banerjee, J. Appl. Phys. **112**, 124511 (2012).
[18]M. Esslinger, R. Vogelgesang, N. Talebi, W. Khunsin, P. Gehring, S. De Zuani, B. Gompf, and K. Kern, ACS Photonics **1**, 1285 (2014).
[19]K. Majhi, K. Pal, H. Lohani, A. Banerjee, P. Mishra, A. K. Yadav, R. Ganesan, B. R. Sekhar, U. V. Waghmare, and P. S. Anil Kumar, Appl. Phys. Lett. **110**, 162102 (2017).
[20]M. Samanta and K. Biswas, Chem. Mater. **32**, 8819 (2020).
[21]M. Samanta, K. Pal, P. Pal, U. V. Waghmare, and K. Biswas, J. Am. Chem. Soc. **140**, 5866 (2018).
[22]R. Starko-Bowes, J. Atkinson, W. Newman, H. Hu, T. Kallos, G. Palikaras, R. Fedosejevs, S. Pramanik, and Z. Jacob, J. Opt. Soc. Am. B **32**, 2074 (2015).

[23]S. Molesky and Z. Jacob, Opt. Express **21**, A96 (2013).
[24]Y. H. Choi, N. H. Jo, K. J. Lee, H. W. Lee, Y. H. Jo, J. Kajino, T. Takabatake, K. T. Ko, J. H. Park, and M. H. Jung, Appl. Phys. Lett. **101**, 152103 (2012).
[25]H. Lind, S. Lidin, and U. Häussermann, Phys. Rev. B **72**, 184101 (2005).
[26]T. Zhu, P. E. Trevisanutto, T. C. Asmara, L. Xu, Y. P. Feng, and A. Rusydi, Phys. Rev. B **98**, 235115 (2018).
[27]T. J. Whitcher, M. G. Silly, M. Yang, P. K. Das, D. Peyrot, X. Chi, M. Eddrief, J. Moon, S. Oh, A. H. Castro-Neto, M. B. H. Breese, A. T. S. Wee, F. Silly, and A. Rusydi, NPG Asia Mater. **12**, 37 (2020).
[28]P. B. Johnson and R. W. Christy, Phys. Rev. B **6**, 4370 (1972).
[29]K. C. Maurya, V. M. Shalaev, A. Boltasseva, and B. Saha, Opt. Mater. Express **10**, 2679 (2020).
[30]G. V. Naik, V. M. Shalaev, and A. Boltasseva, Adv. Mater. **25**, 3264 (2013).
[31]M. Ruzi, C. Ennis, and E. G. Robertson, AIP Adv. **7**, 015042 (2017).
[32]W. Zhang, R. Yu, H. J. Zhang, X. Dai, and Z. Fang, New J. Phys. **12**, 065013 (2010).
[33]M. S. Dresselhaus, G. Dresselhaus, S. B. Cronin, and A. G. S. Filho, *Solid-State Properties from Bulk to Nano* (Springer, 2018).
[34]Z. Wang, P. Yang, G. Qi, Z. M. Zhang, and P. Cheng, J. Appl. Phys. **127**, 233102 (2020).
[35]G. Palermo, K. V. Sreekanth, N. Maccaferri, G. E. Lio, G. Nicoletta, F. De Angelis, M. Hinczewski, and G. Strangi, Nanophotonics **10**, 295 (2020).
[36]G. Ctistis, E. Yuce, A. Hartsuiker, J. Claudon, M. Bazin, J. M. Ǵrard, and W. L. Vos, Appl. Phys. Lett. **98**, 161114 (2011).
[37]T. Nordmann, A. Didier, M. Doležal, P. Balling, T. Burgermeister, and T. E. Mehlstäubler, Rev. Sci. Instrum. **91**, 111301 (2020).
[38]S. A. Diddams, K. Vahala, and T. Udem, Science **369**, eaay3676 (2020).
[39]N. Kinsey, C. DeVault, A. Boltasseva, and V. M. Shalaev, Nat. Rev. Mater. **4**, 742 (2019).
[40]G. Baffou and R. Quidant, Laser Photonics Rev. **7**, 171 (2013).
[41]M. L. Brongersma, N. J. Halas, and P. Nordlander, Nat. Nanotechnol. **10**, 25 (2015).
[42]J. C. Ndukaife, A. V. Kildishev, A. G. A. Nnanna, V. M. Shalaev, S. T. Wereley, and A. Boltasseva, Nat. Nanotechnol. **11**, 53 (2016).
[43]N. Engheta, Science **317**, 1698 (2007).
[44]M. Silveirinha and N. Engheta, Phys. Rev. Lett. **97**, 157403 (2006).
[45]D. C. Adams, S. Inampudi, T. Ribaudo, D. Slocum, S. Vangala, N. A. Kuhta, W. D. Goodhue, V. A. Podolskiy, and D. Wasserman, Phys. Rev. Lett. **107**, 133901 (2011).
[46]S. Campione, J. R. Wendt, G. A. Keeler, and T. S. Luk, ACS Photonics **3**, 293 (2016).
[47]J. Sun, J. Zhou, B. Li, and F. Kang, Appl. Phys. Lett. **98**, 101901 (2011).
[48]S. Dai, Z. Fei, Q. Ma, A. S. Rodin, M. Wagner, A. S. McLeod, M. K. Liu, W. Gannett, W. Regan, K. Watanabe, T. Taniguchi, M. Thiemens, G. Dominguez, A. H. Castro Neto, A. Zettl, F. Keilmann, P. Jarillo-Herrero, M. M. Fogler, and D. N. Basov, Science **343**, 1125 (2014).
[49]J. Sun, N. M. Litchinitser, and J. Zhou, ACS Photonics **1**, 293 (2014).